Sustainable Structures
ISSN: 2789-3111 (Print); ISSN: 2789-312X (Online)
http://www.sustain-dpl.com/journal/sust
DOI: 10.54113/j.sust.2025.000089

ORIGINAL ARTICLE

Advancing sustainable composite flooring: cold-formed steel and timber systems for residential and mid-rise applications

Dheeraj Karki, Harry Far*

School of Civil and Environmental Engineering, Faculty of Engineering and Information Technology, University of Technology Sydney (UTS), Sydney, Australia
*Corresponding author: Harry Far, Email: Harry.Far@uts.edu.au

Abstract: This paper introduces and verifies advanced three-dimensional finite element (FE) models for lightweight composite flooring systems composed of cold-formed steel (CFS) joists combined with structural plywood sheathing. The numerical models, developed in ANSYS, incorporate both material and geometric nonlinearities, simulate the load–slip response of mechanical fasteners, and include realistic contact definitions to capture the interaction between different components. The models were rigorously benchmarked against full-scale experimental tests, demonstrating strong agreement in terms of load–deflection behaviour, strain distribution along the section depth, and observed failure mechanisms. Building on this validation, extensive parametric analyses were performed to evaluate the impact of key design parameters, such as joist wall thickness, section depth, and the spacing of shear connectors. The findings confirm that increasing the thickness and depth of the steel joists enhances the flexural stiffness and load capacity of the flooring system, while closer fastener spacing improves composite action and overall structural efficiency. Finally, a simplified design example is provided to illustrate the proposed method for estimating bending resistance and serviceability deflection in such composite floors.

Keywords: Cold-formed steel joists; Timber floorboards; Finite element modelling; Composite floors; Composite action; Failure mode; Ultimate load capacity

1 Introduction

The construction industry has increasingly adopted modular approaches in recent years due to their distinct advantages over traditional building techniques. Prefabricated modular systems enable faster and safer assembly, improved quality control, reduced material waste, and enhanced sustainability outcomes for the built environment [1, 2]. Hybrid structural systems, which integrate different materials to optimise performance, have become particularly prominent, especially when assembled on-site as modular prefabricated elements [3, 4]. By combining complementary materials in components such as floors, walls, or roofs, hybrid or composite systems achieve structural behaviour superior to that of their individual constituents [5, 6]. Widely recognised examples include composite floors utilising hot-rolled steel and concrete[7, 8], timber and concrete [9, 10], as well as steel and timber combinations[11, 12], all of which have well-established design practices.

For lightweight flooring applications, cold-formed steel (CFS) joists paired with timber sheathing have emerged as an efficient solution [13, 14]. Previous studies, such as those by Zhou et al. [13],

Received: 24 December 2024; Received in revised form: 4 August 2025; Accepted: 29 August 2025

Kyvelou et al. [15], [16], have demonstrated that recognising the composite action at the steel–timber interface significantly improves the structural performance of these systems. Further experimental investigations [14, 17] have highlighted that vibration characteristics can be enhanced by optimising joist support conditions, reducing fastener spacing, and refining construction details such as bridging and blocking. CFS members, typically mono-symmetric thin-walled C-sections, have therefore gained popularity as floor joists and bearers due to their light weight and ease of fabrication[18].

The evolution of engineered timber products—such as oriented strand board (OSB), structural plywood, laminated veneer lumber (LVL), and cross-laminated timber (CLT)—has provided a range of viable options for floor sheathing. These products can be mechanically connected to CFS joists using various fasteners, including self-drilling screws, bolts, and coach screws, depending on regional availability [19, 20]. Cold-formed steel–timber (CFST) composite flooring systems thus present a durable and cost-effective option for addressing housing demands. They allow for mass production, simplified transportation, and rapid on-site assembly while maintaining a high strength-to-weight ratio [6, 21, 22].

This study develops and validates three-dimensional finite element models (FEMs) of CFST composite flooring systems against experimental data. As laboratory testing alone can be time-intensive and costly, the validated FEMs are subsequently employed for parametric analyses to examine the influence of key design parameters on structural performance.

2 Overview of The Experimental Study

As part of this research, thirteen full-scale composite specimens were fabricated and tested to evaluate the flexural performance of cold-formed steel–timber (CFST) flooring systems. Preliminary material characterisation was carried out for both the CFS joists and the plywood panels to determine their fundamental mechanical properties. Additionally, push-out tests were performed to establish the load–slip relationships of the mechanical fasteners used as shear connectors in the composite beams. Comprehensive details of the material tests and push-out procedures are available in previously published studies [23, 24]. The general experimental arrangement for the four-point bending tests is depicted in **Fig. 1**.

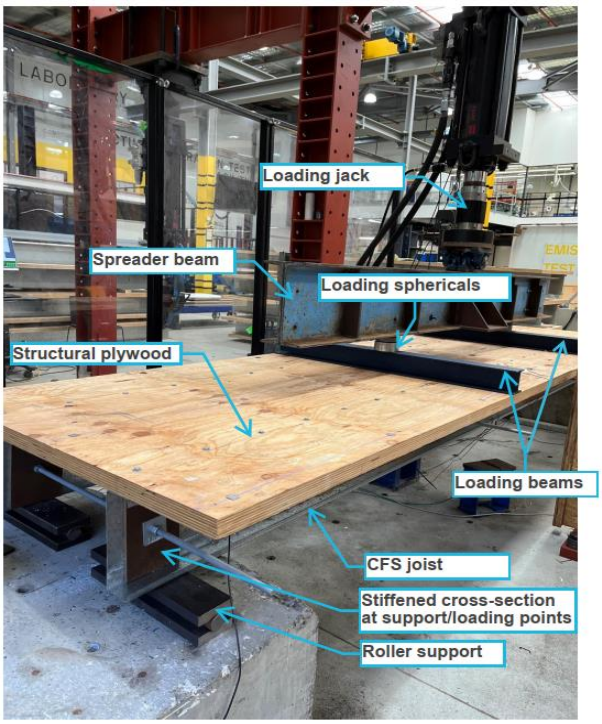

Fig. 1. Experimental setup for four-point bending configuration used for testing the composite beams

Each specimen consisted of a pair of CFS C-section joists placed back-to-back at a clear spacing of 600 mm, sheathed with structural plywood panels attached using various types of shear connectors at different intervals. The test beams were simply supported over a clear span of 4.5 m, with an additional 100 mm overhang beyond each support. To capture the global and local responses during testing, four linear variable displacement transducers (LVDTs) were installed at the beam ends to measure longitudinal slip between the steel and plywood. Vertical deflections at critical points beneath each joist were monitored using string potentiometers. Furthermore, strain gauges were mounted across the height and width of the midspan cross-section to record strain distribution and identify the neutral axis position within the composite section. Loading was applied using a 500 kN MTS hydraulic actuator, with the force distributed evenly to the width of the plywood via a spreader beam connected to two transverse loading beams. To prevent local web distortion at the support and loading points, 12 mm thick Grade 350 steel plates were clamped on either side of the joist webs using M16 Grade 8.8 threaded rods. This local reinforcement ensured a more uniform transfer of concentrated loads. A summary of the specimens and the key outcomes of the four-point bending tests is provided in Table 1. More detailed descriptions of the test setup and methodology are available in related publications [25].

Table 1. An overview of the composite beam specimens and highlights the principal results obtained from the four-point bending experiments

Specimen	Web hole in joist	Type of shear connection	Spacing of shear connection (mm)	Structural adhesive at beam-board interface	Ultimate load (kN)	Mid-span deflection at ultimate load (mm)
SP-1	No	NA	NA	NA	54	37
SP-2	No	Self-drilling screw	400	No	58.2	36.5
SP-3	No	Self-drilling screw	200	No	70	43.6
SP-4	No	Self-drilling screw	400	Yes	63.8	36.6
SP-5	No	M 12 Coach screw	400	No	84.6	53.8
SP-6	No	M 12 Coach screw	200	No	87.85	47.1
SP-7	No	M12 nut and Bolt	400	No	86.6	57.1
SP-8	No	M12 nut and Bolt	800	No	72.1	46.8
SP-9	No	M12 nut and Bolt	800	Yes	80	50.5
SP-10	No	M8 nut and Bolt	200	No	85.8	53
SP-11	No	M8 nut and Bolt	400	No	81	52.2
SP-12	Yes	M12 nut and Bolt	800	No	71	44.2
SP-13	Yes	M 12 Coach screw	200	No	86	44
SP-14	No	M12 Coach screw	400	Yes	83.8	52

3 Development of Finite Element Models

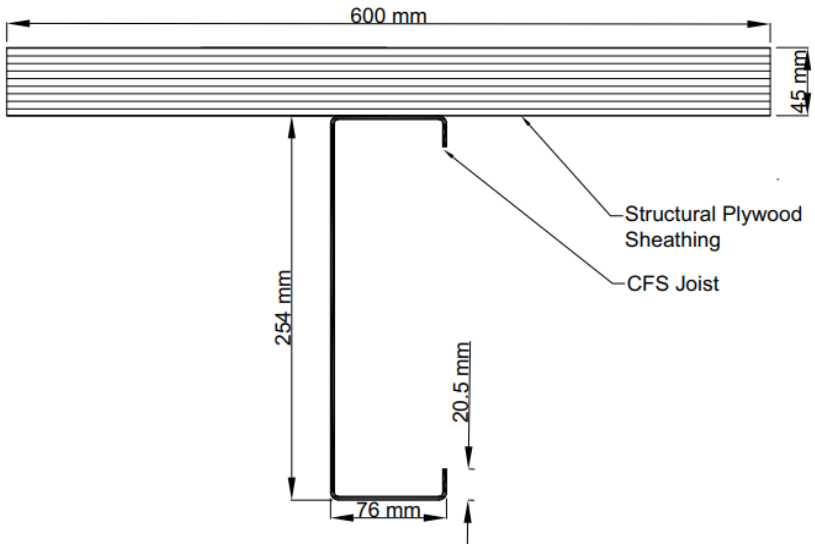

Fig. 2. Cross-sectional configuration of the CFST composite beam adopted for finite element model validation

Numerical simulations were carried out using the ANSYS finite element software package[26], which has been widely applied in the analysis of cold-formed steel components[13, 27, 28]. The models were designed to replicate the behaviour of the full-scale composite beams described in Section 2. While the experimental setup featured two CFS joists spaced 600 mm apart, the numerical model simplified the system by representing a single joist combined with an equivalent effective width of the plywood sheathing, as illustrated in **Fig. 2**. Appropriate boundary conditions were applied to capture the actual support and loading configurations.

This section outlines the essential modelling strategies, including the adopted material properties, element types, meshing approaches, and contact definitions. These features form the basis for the subsequent validation of the finite element models against experimental results, followed by a series of parametric studies to examine the influence of key design parameters.

3.1 Material inputs

Accurate representation of material properties is essential for finite element models to reliably simulate the structural response of composite systems. Mechanical characteristics of both the cold-formed steel (CFS) joists and the structural plywood panels were determined through material testing and incorporated into the numerical analysis.

3.1.1 Cold-formed steel material modelling

he CFS material exhibited a multi-linear stress–strain response under uniaxial tensile loading. Fig. 3 presents the averaged stress–strain relationship, while **Table 2** summarises the key mechanical properties obtained from tensile coupon tests. For use in ANSYS shell elements, the nominal stresses (σ) and strains (ε) measured in these tests were converted into true stresses and strains using the well-known transformation equations (1) and (2) [16, 26].

$$\sigma_{true} = \sigma\left(1+\varepsilon\right) \quad (1)$$

$$\varepsilon_{\text{true}} = \ln\left(1+\varepsilon\right) - \sigma_{\text{true}} / E \quad (2)$$

Table 2. Key material properties of cold-formed steel utilised in model calibration and subsequent parametric analyses

Thickness, t (mm)	Height (mm)	Flange width (mm)	Elastic modulus (MPa)	Yield strength (MPa)	Tensile strength (MPa)
2.4	254	76	207000	504	567

The material behaviour in the FE models was defined using the Von Mises yield criterion with associative flow rules and isotropic hardening. This approach assumes uniform plastic deformation under monotonic loading, which aligns with the expected structural response in this study. Although cold-formed steel inherently displays some anisotropy due to the manufacturing process, isotropic hardening is widely adopted in similar numerical investigations and provides conservative predictions for global behaviour [13]. Since CFS typically lacks a distinct yield plateau in its stress–strain curve, the yield stress (f_y) was defined as the 0.2% proof stress, in line with previous research [27, 29]. Residual stresses were neglected in the FE models because their effect on the ultimate bending capacity of CFS members is considered minimal [18, 30]. Furthermore, the material properties were derived directly from coupon tests on the fabricated sections, ensuring that any residual stress effects were implicitly accounted for [16, 31]. Therefore, omitting explicit residual stress modelling did not significantly affect the accuracy of strength predictions.

3.1.2 Plywood material modelling

The plywood panels were modelled as an equivalent homogeneous material, given the relatively small thickness of individual laminations. The constitutive behaviour of the plywood was defined as an idealised elastic–plastic relationship, as illustrated in **Fig. 4** and based on the formulation in [32]. Although plywood is inherently orthotropic, for simplicity the mechanical properties were assumed identical in all directions in the FE model. Material properties derived from previous experimental studies [23, 24] were adopted. As summarised in Table 3, the plywood sheathing exhibited an average

bending yield strength of 17 MPa and a modulus of elasticity of 10,000 MPa. A Poisson's ratio of 0.3 was assumed in accordance with published data [33].

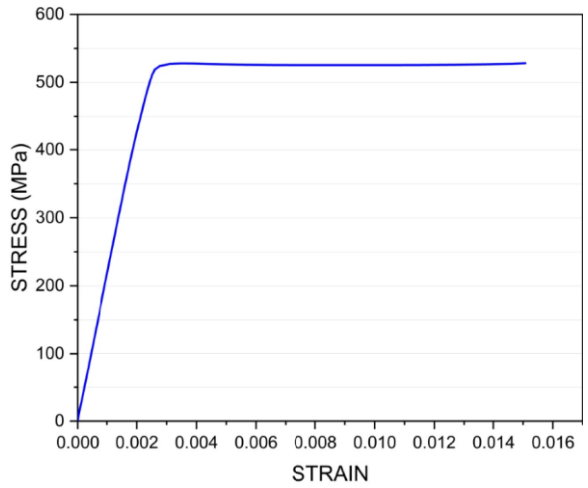

Fig. 3. Average of stress-strain data obtained from CFS tensile test

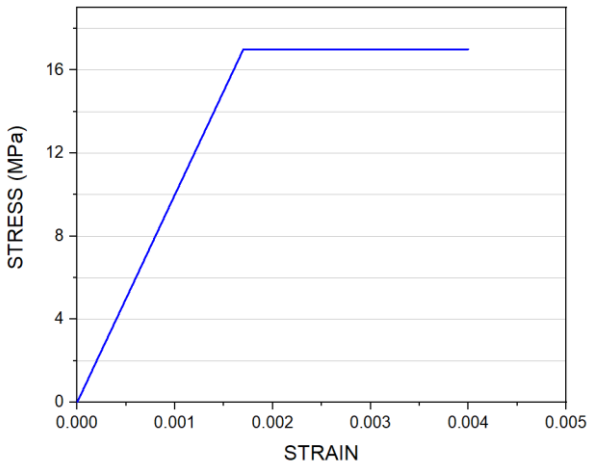

Fig. 4. Elastoplastic model adopted for plywood in FE model

Table 3. Mechanical characteristics of structural plywood (MPa) utilised for model verification and parametric analysis

Bending parallel to grain ($f_{b,0}$)	Bending perpendicular to grain ($f_{b,90}$)	Tension parallel to grain ($f_{t,0}$)	Tension perpendicular to grain ($f_{t,90}$)	Compression parallel to grain ($f_{c,0}$)	Compression perpendicular to grain ($f_{c,90}$)	Modulus of Elasticity (E)
40	45.5	22	17	31.5	28	10000

3.2 Element selection and mesh configuration

Cold-formed steel (CFS) joists were represented using the SHELL181 finite element, a choice supported by multiple prior investigations[27, 34, 35] demonstrating its effectiveness in replicating the experimental behaviour of CFS structures. SHELL181 is a quadrilateral element featuring four nodes, each possessing six degrees of freedom, including translations and rotations along the x, y, and z axes. This element is capable of modelling substantial plastic deformations and is well-suited for non-linear analyses involving thin to moderately thick shell-like components. For the structural plywood panels, SOLID185 elements were employed to model the three-dimensional solid behaviour. These elements have eight nodes with three translational degrees of freedom per node (along x, y, and z directions) and support large strain and large deflection analyses.

The precision of the finite element model critically depends on the choice of mesh density. To ensure accurate results while maintaining computational efficiency, a mapped meshing strategy was adopted, generating a uniform mesh with well-shaped elements. In the current simulations, the cross-sectional area was discretised into 132 solid elements representing plywood and 62 shell elements for the steel joists. Along the longitudinal axis, mesh sizes were assigned as 10 mm for the shell elements and 20 mm for the solid elements.

3.3 Representation of fasteners and contact interfaces

The shear connections linking the plywood panels to the cold-formed steel (CFS) joists were established using a range of mechanical fasteners: 6 mm diameter self-drilling screws (Size 14), M8 nuts and bolts, M12 coach screws, and M12 nuts and bolts. To model these connections, the COMBIN39 element—a nonlinear, unidirectional spring capable of representing complex force–displacement behaviour—was employed. The characteristic load versus slip data for these fasteners, obtained experimentally by Karki et al. [23] through push-out testing, informed the definition of the spring behaviour in the finite element analysis. **Fig. 5**. illustrates the load-slip curves implemented in the nonlinear spring elements corresponding to each type of shear connection.

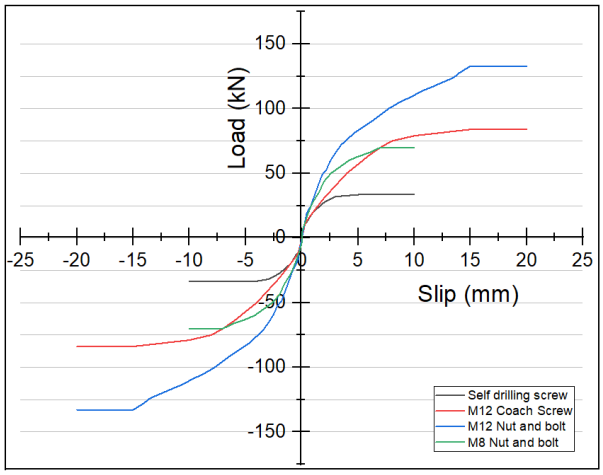

Fig. 5. Load versus slip curves applied to nonlinear spring elements representing various fastener types

The interaction between the underside of the plywood sheathing and the top flange of the cold-formed steel (CFS) joists was modelled using surface-to-surface contact pairs. Specifically, the CONTA174 and TARGE170 elements were selected to represent the contact and target surfaces, respectively. In this setup, the plywood's lower face served as the contact surface, while the upper flange of the CFS joist was designated as the target surface, as depicted in **Fig. 6**. These elements correspond geometrically to the faces of the adjoining solid or shell elements. The contact behaviour was assumed to follow a standard model, with a Coulomb friction coefficient of 0.35 applied to represent the isotropic friction between the steel and timber interfaces [32].

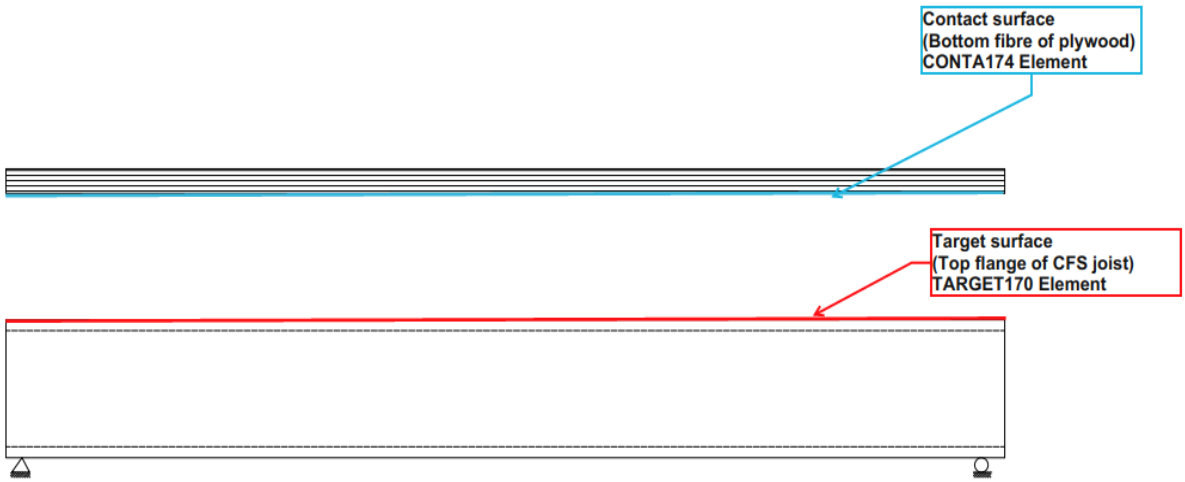

Fig. 6. Diagram illustrating the contact and target surfaces in the finite element model of the CFST beam

3.4 Loading and support conditions

The experimental configuration involved a composite CFST beam measuring 4700 mm in length, simply supported over a 4500 mm span. To avoid local instability and web failure at points of concentrated load and support, these regions were reinforced in the physical tests. Reflecting this in the finite element analysis, rigid plates were attached to the CFS joists at the loading and support locations, with the plates assigned an artificially elevated elastic modulus set at ten times that of the steel material. Vertical and lateral (out-of-plane) displacements were restrained at both supports, and to eliminate rigid body movement, one support was fixed in the longitudinal direction. Due to the symmetry of the specimens, only half of the beam cross-section—illustrated in **Fig. 2**—was modelled, applying symmetric boundary conditions along the axis to optimise computational efficiency. Two concentrated vertical loads, each corresponding to half the total applied load (P/2), were imposed at one-third and two-thirds of the span length, generating a region of pure bending between these loads. Fig. 7 presents

a schematic of the four-point bending test setup, while Fig. 8 provides an overall view of the model geometry and boundary constraints.

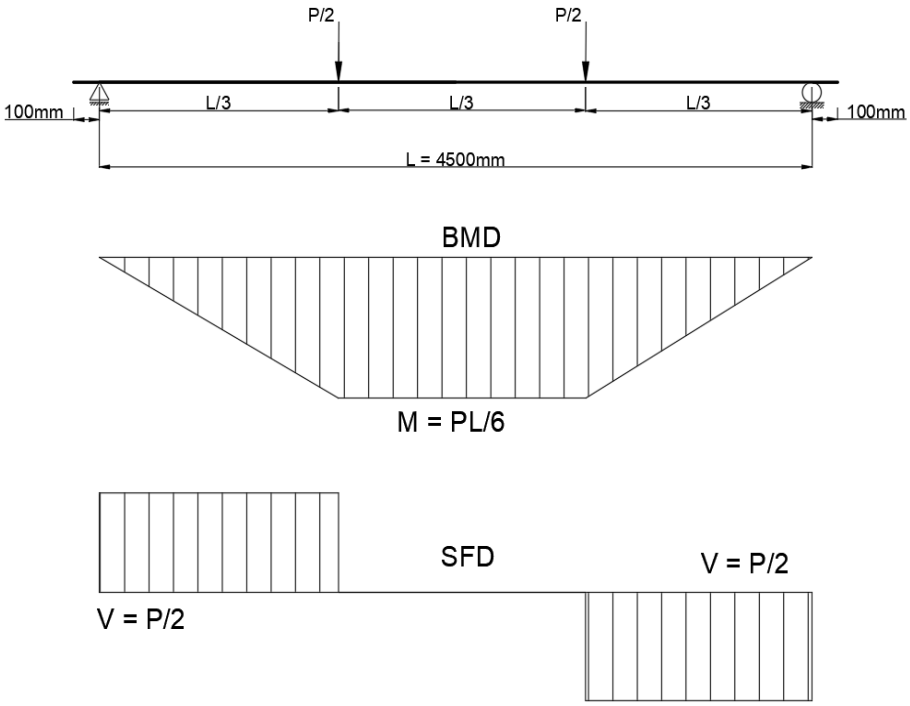

Fig. 7. Simplified finite element representation of the four-point bending test

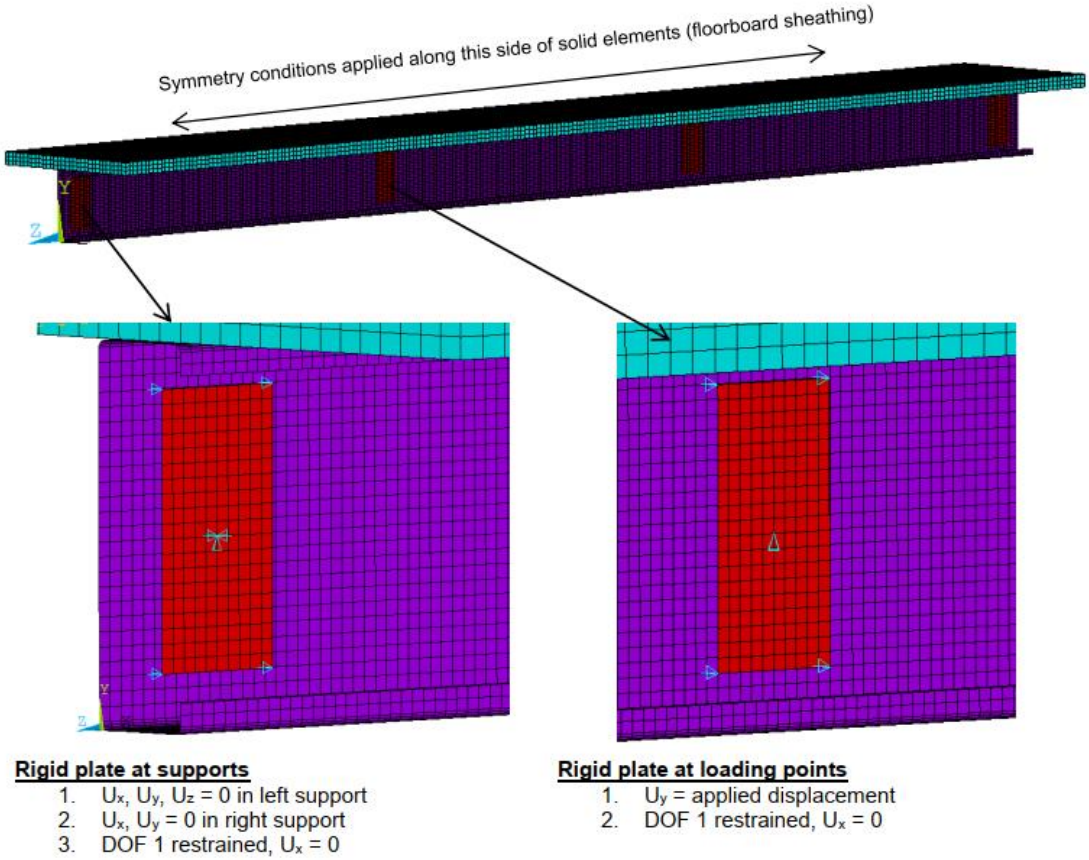

Fig. 8. Boundary condition setup applied in the finite element model for numerical simulation

3.5 Analysis assumptions

The analyses conducted in this study utilised a nonlinear solution approach based on the Newton-Raphson iterative method. A large displacement static analysis was implemented, accounting for both material and geometric nonlinearities. Loading was applied incrementally through multiple steps following a displacement-controlled scheme. Due to the complexities introduced by significant deformations, nonlinear material responses, and extensive contact interactions, achieving numerical convergence was challenging throughout the simulations. To address these difficulties, a nonlinear stabilisation method was employed, with multi-step restarts used to facilitate stable convergence.

4 Validation of Finite Element Models

The reliability of the finite element models developed in this research was established through comparison with experimental data obtained from four-point bending tests. Table 1 summarises the physical testing of thirteen composite beam specimens, each featuring different shear connection types, alongside a bare steel beam, all simply supported over a 4500 mm span. For validation purposes, five of these composite configurations were selected for detailed numerical comparison. Specifically, one specimen from each of the four shear connection categories at 400 mm spacing was chosen: SP-2 (self-drilling screws at 400 mm), SP-5 (coach screws at 400 mm), SP-7 (M12 nuts and bolts at 400 mm), and SP-11 (M8 nuts and bolts at 400 mm). Additionally, SP-3, which employs self-drilling screws spaced at 200 mm, was included to assess the model's accuracy for closer fastener spacing.

The comparisons between the ultimate moment capacities $M_{u,exp}$ and flexural stiffness $(EI)_{exp}$ obtained from experimental testing, and those predicted by finite element models $M_{u,fea}$ and $(EI)_{fea}$ are presented in Table 4. The average ratios of experimental to predicted ultimate moment and stiffness were found to be 0.98 and 0.97, respectively, indicating strong agreement between the models and physical tests.

Table 4. Overview of finite element predictions versus experimental test outcomes

Specimen	$M_{u,fea}/ M_{u,exp}$	$(EI)_{fea}/(EI)_{exp}$
SP-2	1.02	0.99
SP-3	1.05	1.02
SP-5	0.96	0.965
SP-7	0.95	0.91
SP-11	1.02	1.01
Mean	0.98	0.97

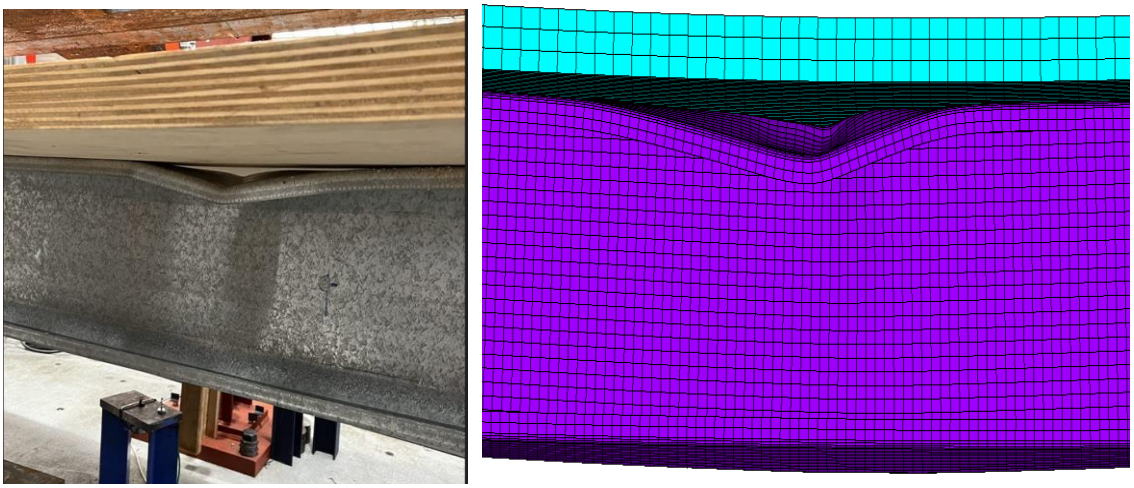

(a) Test (b) Finite element analysis

Fig.9. Typical observed failure mode of specimen SP-11

The failure mechanisms predicted by the finite element models are demonstrated in **Fig. 9**. All specimens with shear connectors spaced at 400 mm experienced in-plane failure within the constant moment zone, characterised by distortional buckling of the CFS joist's top flange between the fasteners.

The finite element analysis results for load-deflection behaviour and strain patterns at peak load closely matched those observed in the physical experiments, as depicted in **Fig. 10** and **11**, respectively.

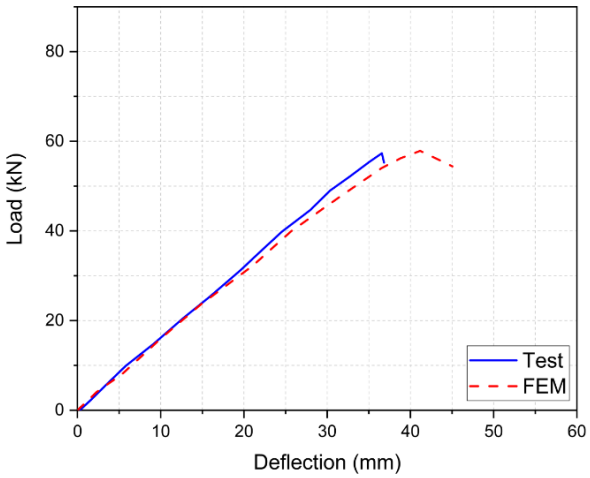

(a) Specimen SP-2 (SDS at 400 mm)

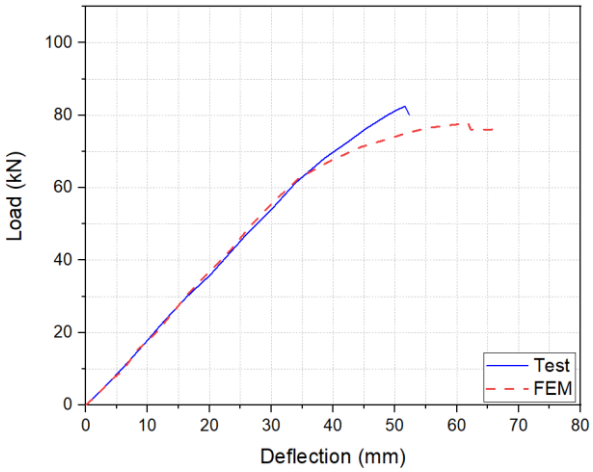

(b) SP-11 (M8 NB at 400 mm)

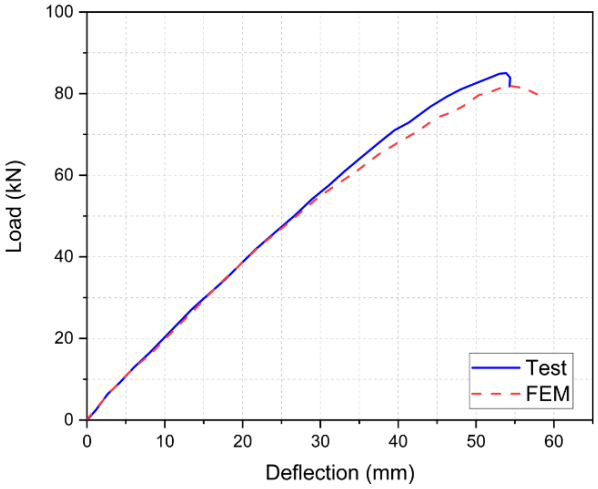

(c) SP-5 (M12 CS at 400 mm)

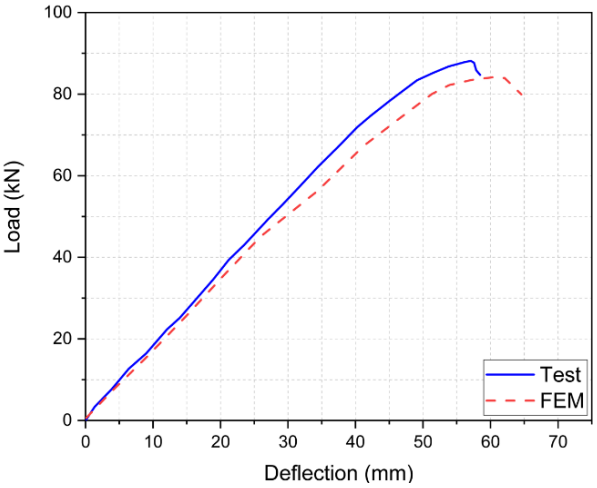

(d) SP-7 (M12 NB at 400 mm)

Fig.10. Load-deflection responses of specimens: experimental results versus finite element predictions

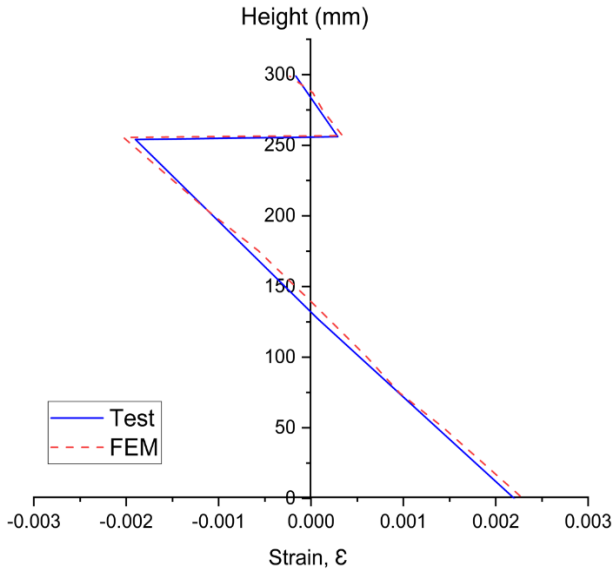

（a）SP-3 (SDS at 200 mm)

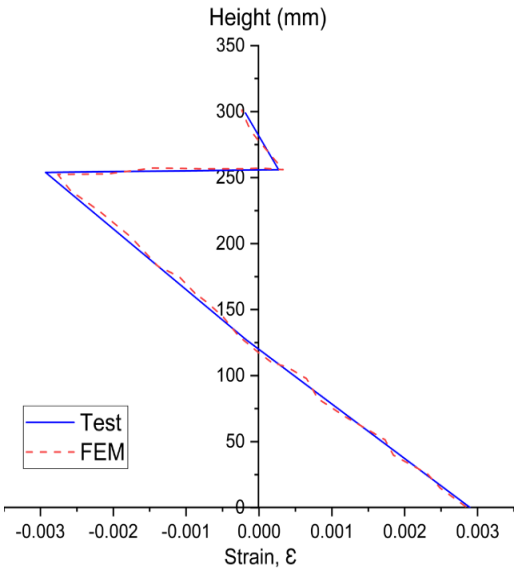

(b)SP-11 (M8 NB at 400 mm)

Fig.11. Comparison of cross-sectional strain profiles at ultimate load: experimental measurements and finite element results

Following successful validation, the established finite element models were employed to explore additional factors influencing the performance and load-bearing capacity of the composite CFST beams. Throughout these analyses, the characteristic bending failure mode involving distortional buckling of the CFS joist flange between fasteners, along with the associated von Mises stress distribution, is illustrated in **Fig. 12**.

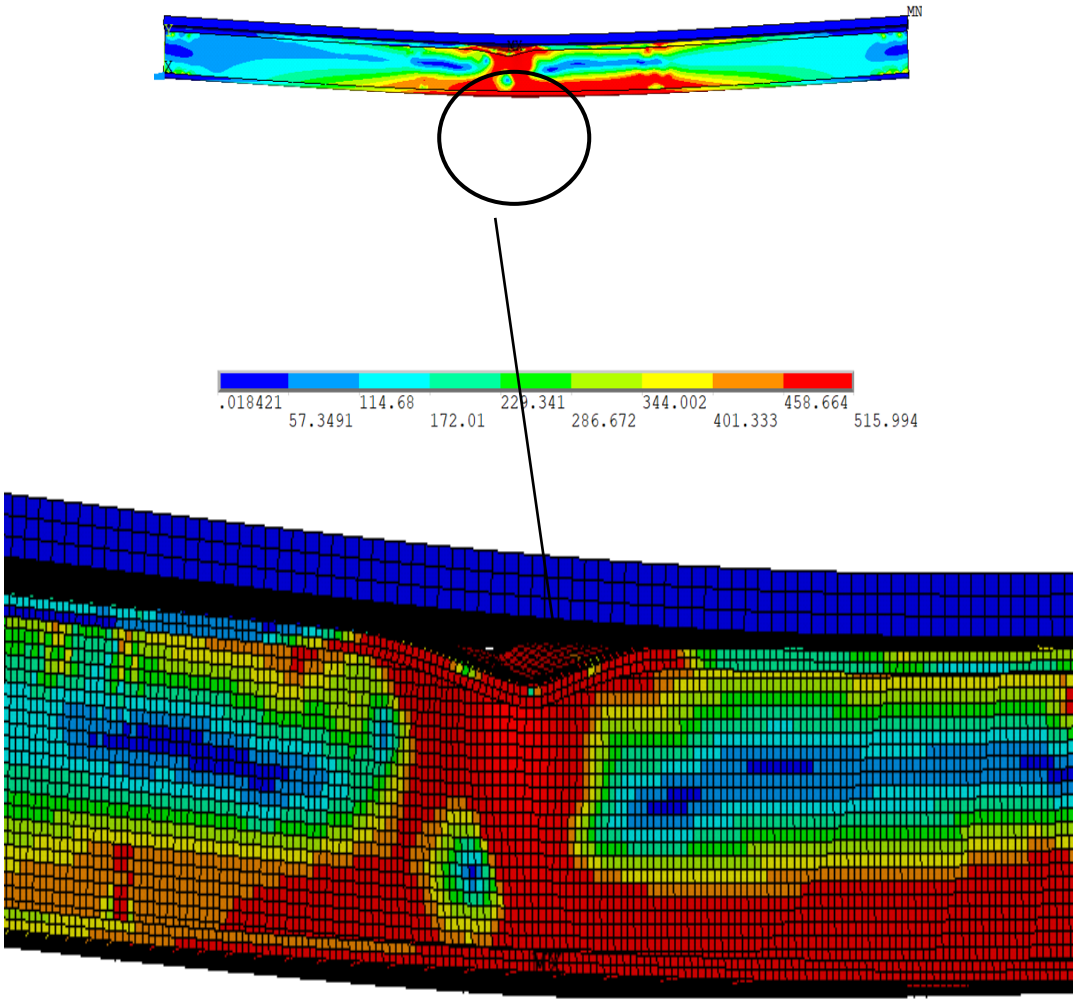

Fig.12. Characteristic bending failure at midspan showing distortional buckling between fasteners

5 Parametric investigation and results analysis

A series of parametric analyses were performed to assess how variations in cold-formed steel (CFS) joist thickness, depth, and fastener spacing affect the structural behaviour of composite floor systems consisting of CFS joists and structural plywood sheathing. The focus was on ultimate bending strength, flexural rigidity, and the extent of composite interaction achieved. For consistency, the load-deflection characteristics of M8 bolts were applied across all parametric scenarios.

5.1 Effect of CFS joist thickness

Three different CFS joist thicknesses commonly used in construction—1.5 mm, 2.0 mm, and 3.0 mm—were selected for evaluation. Apart from the thickness, all other geometric properties of the CFS sections matched those employed in the composite beam experiments. The specimen with 1.5 mm thickness is designated as C25015, where ‘C’ denotes the cold-formed steel section and ‘250’ refers to the web depth in millimetres. The finite element parametric study results illustrating the influence of joist thickness on the bending capacity of composite CFST beams are summarised in **Fig. 13** and **Table 5**.

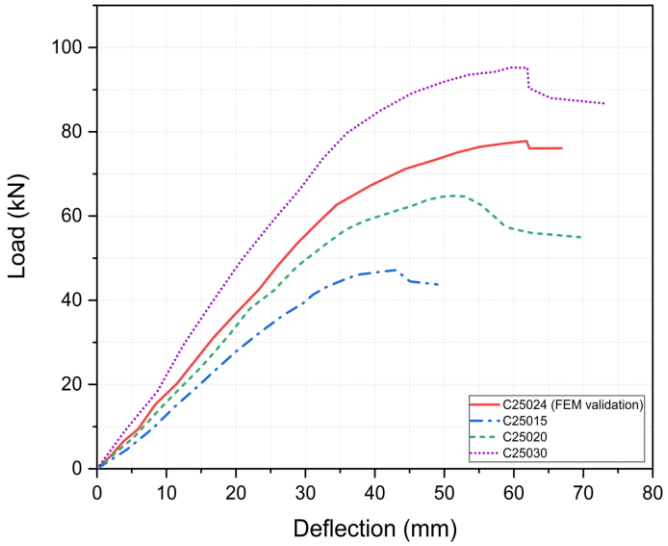

Fig.13. Load versus deflection behaviour of specimens varying in CFS joist thickness

Table 5. Effect of cold-formed steel joist thickness on bending strength and stiffness of composite CFST beams

Numerical specimens	CFS joist thickness (mm)	Predicted ultimate moment capacity, M_u (kN.m)	Predicted flexural stiffness under service load (N.m^2)
C25015	1.5	35.36	2.33×106
C25020	2.0	48.45	2.74×106
C25024	2.4	58.35	2.9×106
C25030	3.0	71.4	3.72×106

An increase in the thickness of the CFS section corresponded to a near-linear improvement in the load-carrying capacity of the composite beams. Specifically, raising the joist thickness from 1.5 mm to 2.0 mm, then from 2.0 mm to 2.4 mm, and subsequently from 2.4 mm to 3.0 mm led to increases in bending strength of approximately 37%, 20.5%, and 23%, respectively. In parallel, the estimated flexural stiffness of the composite CFST beams rose by about 18%, 7%, and 28% for the same thickness increments. The gains in structural performance are attributed to increases in the section modulus and moment of inertia resulting from the thicker CFS profiles, which enhanced both the ultimate bending moment and the flexural rigidity. Additionally, the greater thickness improved the steel joist's resistance against flange buckling, thereby elevating the overall load-bearing capacity of the composite system.

5.2 Effect of CFS web depth

In this investigation, all geometric and material parameters of the cold-formed steel sections remained constant except for the web height. Three commercially available CFS profiles with web depths of 150 mm, 200 mm, and 300 mm were selected to evaluate the impact of web height on the structural behaviour of composite CFST floor systems. The finite element analysis outcomes for bending capacity and flexural rigidity corresponding to these varying web heights are summarised in **Table 6**. As anticipated, increasing the depth of the joist notably enhanced both stiffness and load-bearing capacity, as demonstrated in **Fig. 14**. For instance, elevating the web height from 150 mm to 250 mm yielded increases in ultimate moment capacity and bending stiffness of approximately 87% and 190%, respectively. This improvement aligns with fundamental principles of mechanics of materials, where a deeper section leads to a larger moment of inertia, thereby producing stronger beams with significantly improved flexural performance.

Table 6. Effect of cold-formed steel web height on bending strength and stiffness of composite CFST beams

Numerical specimens	CFS web height (mm)	Predicted ultimate moment capacity, M_u (kN.m)	Predicted flexural stiffness under service load (N.m^2)
C15024	150	31.2	0.99×106
C20024	200	44.55	1.73×106
C25024	250	58.35	2.9×106
C30024	300	70.12	2.33×106

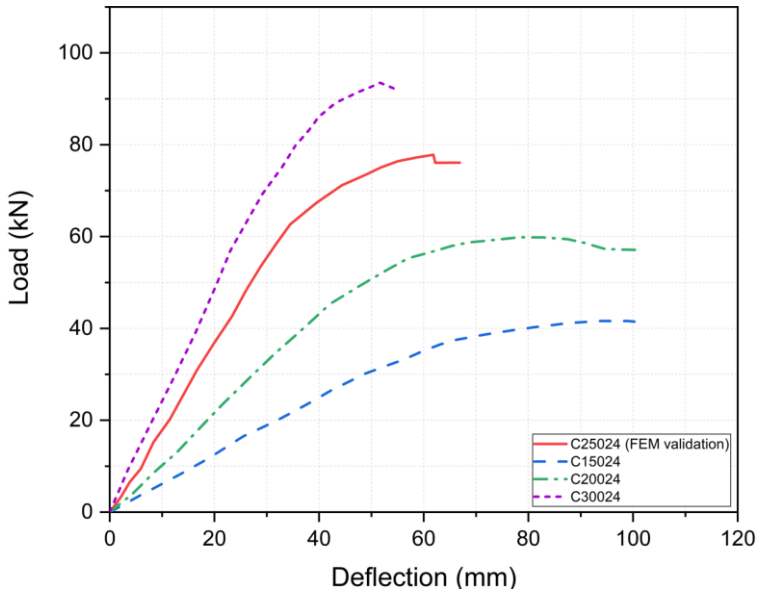

Fig.14. Load-deflection behaviour of specimens with varying CFS web depths

5.3 Effect of fastener spacing

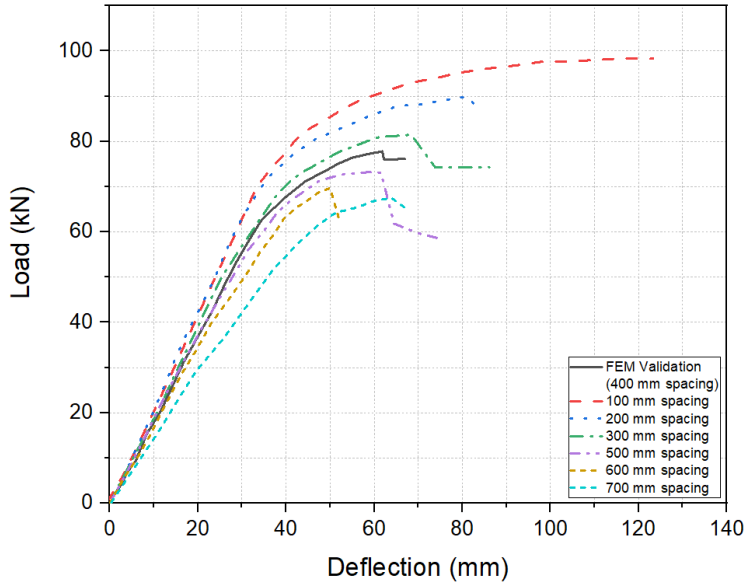

Fig.15. Load–deflection curves of specimens with varying fastener spacings

Table 7. Effect of fastener spacing on bending strength and stiffness of composite CFST beams

Fastener spacing (mm)	Predicted ultimate moment capacity, M_u (kN.m)	Predicted stiffness under service load (N.m^2)
100	73.5	3.3 ×106
200	66.5	3.3×106
300	61.2	3.11×106
400	58.35	2.9×106
500	54.8	2.86×106
600	52.2	2.65×106
700	50.6	2.3 ×106

Experimental studies have examined the impact of fastener spacings at 200 mm, 400 mm, and 800 mm across four types of shear connectors. These results provide valuable insights into how different shear connection types and their spacing influence structural behaviour and the limitations of

connection configurations. The experiments revealed that ductile connectors such as M12 coach screws and M12 bolts tend to be limited by yielding of the cold-formed steel, thereby making them less suitable for lightweight cold-formed steel flooring systems. To supplement the existing experimental data and quantify spacing effects further, numerical analyses were conducted for M8 nuts and bolts at spacings of 100 mm, 200 mm, 300 mm, 400 mm, 500 mm, 600 mm, and 700 mm. Reducing the spacing between fasteners reduces slip at the interface between the plywood sheathing and the CFS joist, thereby improving shear transfer and enhancing composite action within the floor system. The finite element predictions for bending capacity and flexural stiffness under varying fastener spacings are summarised in **Fig. 15** and **Table 7**.

Reducing the fastener spacing from 700 mm to 100 mm resulted in increases of approximately 48% in ultimate moment capacity and 43% in flexural stiffness. The effect of varying fastener spacing on the load-bearing capacity of composite CFST beams is illustrated in **Fig.16**.

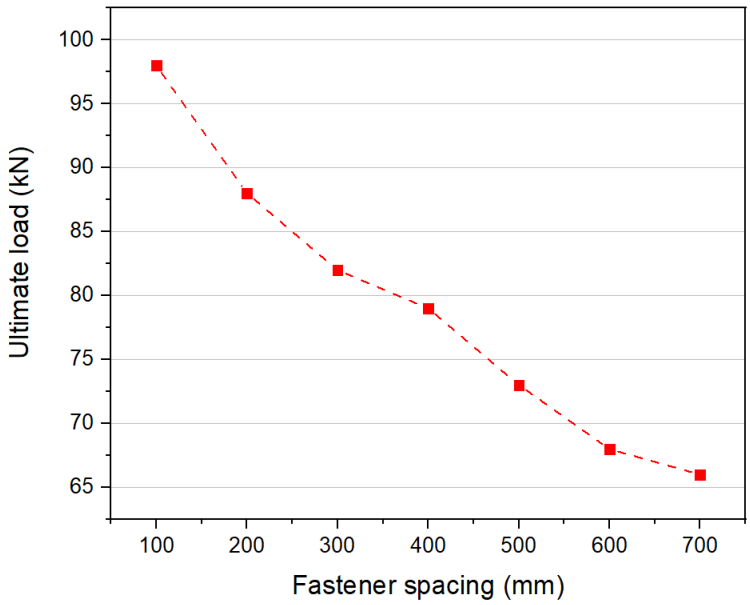

Fig.16. Effect of fastener spacing on the structural capacity of composite CFST beams

The local and distortional buckling wavelengths of the CFS section, as calculated using the finite strip software THINWALL[36], were 140 mm and 600 mm, respectively. **Fig.15** shows that the specimen with 100 mm fastener spacing exhibited higher flexural capacity because this spacing effectively limited local buckling of the top flange, which occurs at a wavelength exceeding 100 mm, thereby enhancing load-carrying performance. When the fastener spacing increased beyond 500 mm to 600 mm and 700 mm, a noticeable reduction in the slope of the load-deflection curve was observed, attributed to the spacing exceeding the distortional buckling wavelength. Shi et al. [37] similarly found that, for self-drilling screw connectors, spacing greater than the distortional buckling wavelength resulted in significant loss of flexural strength. In contrast, this study utilised M8 nuts and bolts, which offer greater ductility than self-drilling screws; consequently, while the moment capacity did not decline sharply, the flexural stiffness of the composite beam decreased markedly.

6 Design of Shear Connectors for Complete shear connection

The design of shear connectors must ensure that mechanical fasteners effectively transfer shear forces between the timber sheathing and the cold-formed steel (CFS) joist, without failure occurring in the fasteners or the connected materials. For composite CFST floors to develop full shear connection, the quantity of fasteners should be sufficient to fully utilise the material strengths and achieve the plastic bending capacity of the system. When the number of fasteners is insufficient, shear transfer is restricted, leading to partial shear connection and a consequent reduction in the ultimate flexural capacity. To clarify the mechanism of shear force transfer, **Fig. 17** presents a free-body diagram of the composite beam along with the floor sheathing section to the left of midspan.

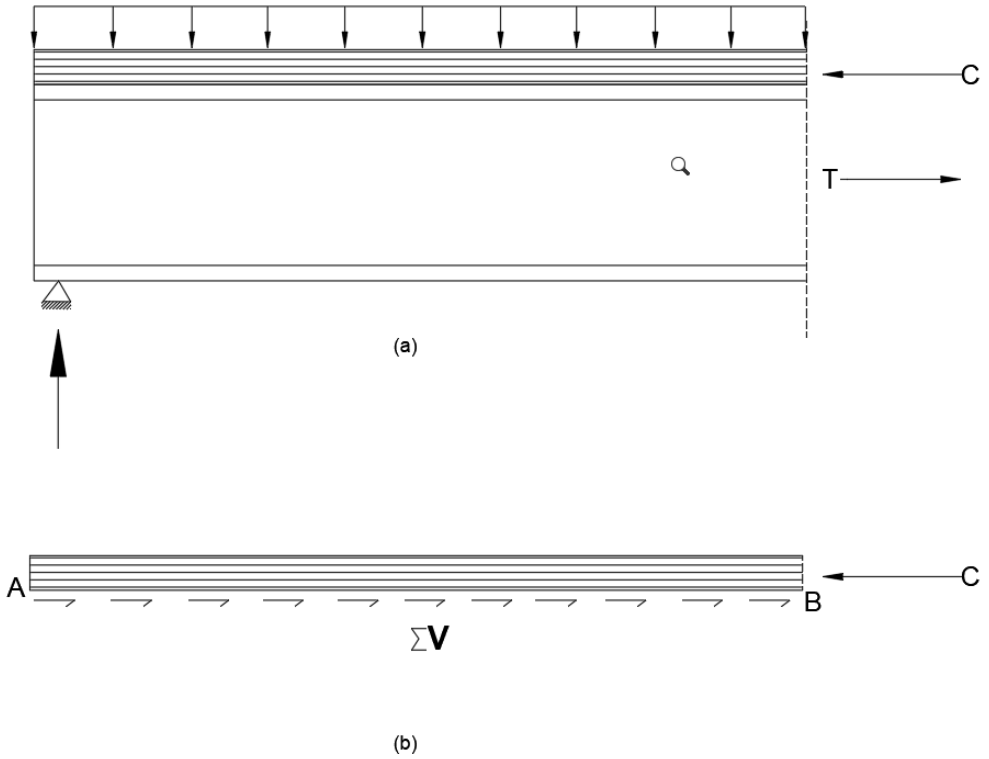

Fig. 17. (a) Free-body diagram of the composite beam segment left of mid-span; (b) free-body diagram of the floor sheathing portion left of mid-span

Considering a horizontal equllibrium of the composite system, from Fig. 6.1 (a) and (b), C=T, and ΣV = C respectively. This equation can be re-written as, C = ΣV = T. As broadly discussed in Chapter 4, the tensile force, T on the CFS joist or compression force, C on the floorboard sheathing can be calculated as per Equations (1) and (2) respectively.

$$T = A_{st} \times f_y \tag{1}$$

$$C = A_b \times f_{cb} \tag{2}$$

Hence, if the shear connection between the timber sheathing and CFS joist is able to transfer the full 'ΣV', complete shear connection is achieved and the full tension 'T' and compression 'C' can be developed. And if the number of fasteners is less than that required, then ΣV < T or C resulting in partial shear connection which is controlled by the resistance of the shear connectors.

Based on the simplified approach outlined in AS2327.1 Composite Structures—Part 1: Simply Supported Beams [38], the longitudinal shear force, *Q*, that the shear connectors in a composite beam can transfer is constrained either by the fastener's shear capacity, V_f, or by the bearing strength of the timber sheathing, V_b. The design shear capacity for each fastener may be determined using Equations (3) and (4), or alternatively derived from push-out test results for the specific fastener used in this study. Notably, Equation (3) aligns with Clause 5.3 of AS/NZS 4600: Cold-formed Steel Structures, which governs the design of pin connections subjected to shear.

$$V_f = \Phi \times 0.62 \times f_{uf} \times n_s \times A_f \tag{3}$$

Where f_{uf} represents the ultimate strength of the fastener,, n_s denotes the number of shear planes, and A_f is the cross-sectional area of the fastener. Similarly, the bearing capacity of the timber sheathing at each fastener location is calculated using Equation (4).

$$V_b = \Phi \times d_f \times t_b \times f_{cb} \tag{4}$$

Where, ϕ = 0.8 is the capacity reduction factor, d_f is the nominal diameter of fastener, t_b is the thickness of floorboard, and f_{cb} is the compressive strength of floorboard. Hence, the magnitude of longitudinal shear force Q is the lesser value of V_f or V_b. For a complete shear connection, the number

of shear connectors n_f required along each critical length of the beam (from mid-span to left or right support) is:

$$n_f = \Sigma V or T / Q \quad (5)$$

Since there are two critical spans requiring number of shear connectors, nf , on either side from mid-span, the total number of shear connectors N_f required along the full length of the beam is:

$$N_f = 2n_f \quad (6)$$

Accordingly, for a flooring system containing nnn shear connectors distributed along the entire span, the degree of shear connection, η is determined as:

$$\eta = n / N_f \leq 1 \quad (7)$$

Comprehensive design standards are well established for hot-rolled steel beams, reinforced concrete slabs, and timber-concrete composite floors. However, appropriate design methodologies for lightweight composite floors using cold-formed steel and timber remain lacking, aside from some preliminary studies showing promising results [39]. The following section presents a simplified design example to illustrate the advantageous impact of composite action on the bending strength of cold-formed steel and timber floor systems.

7 Simplified Calculation Example

Design a flooring system spanning 6.0 m, consisting of G450 cold-formed steel (CFS) joists spaced at 600 mm centres, covered with timber floorboards as illustrated in Fig.18. The system must comply with ultimate limit state (ULS) and serviceability limit state (SLS) criteria. The floor is subjected to a uniform dead load of 2.0 kPa and a live load of 3.0 kPa. Shear connection is provided by M8 nuts and bolts spaced at 300 mm intervals. The mechanical properties and geometric parameters of the steel joists, timber sheathing, and shear connectors are detailed below.

CFS joist description:

Yield strength, F_y = 450 MPa; Elastic modulus, Es = 200,000 MPa; Height, h_s = 200mm; Thickness, t_s = 2.4 mm; Area A_s = 900 mm^2; Second moment of area, $I_s = 5.68 \times 10^6$ mm^4 ; $Z_x = 56.62 \times 10^3$ mm^3

Timber floorboard:

Timber type = F11 grade structural plywood panel; Bending yield strength, F_{by} = 20 MPa; Elastic modulus in bending, E_b = 10,000 MPa Thickness, t_b = 45mm; Effective width, b_{eff} = 600mm; Second moment of area, I_b = 4556250 mm^4

Design loads

Uniformly distributed dead load as line load on each beam, DL = 2.0 ×0.6 = 1.2 kN/m

Uniformly distributed live load as line load on each beam, LL = 3.0 × 0.6 = 1.8 kN/m

For ULS design, the design load is: q^* = 1.2DL + 1.5LL = 1.2 × 1.2 + 1.5 × 1.8 = 4.14 kN/m

For SLS design, the design load is: q_s = 1.0DL + 1.0LL = 1.0 × 1.2 + 1.0 × 1.8 = 3 kN/m

Design bending moment, $M_d = q^*L^2/8$ = 18.63 kN.m

Design shear force, $V_d = q^*L/2$ = 12.42 kN

Attained degree of shear connection

The design shear capacity of the individual fastener and bearing resistance of the timber sheathing are calculated from Equations (3) and (4), respectively:

$V_f = \Phi \times 0.62 \times f_{uf} \times n_s \times A_f$ = 9.9 kN

$V_b = \Phi \times d_f \times t_b \times f_{cb}$ = 8 kN

The magnitude of longitudinal shear force Q is the minimum of V_f or V_b = 8 kN

The longitudinally transferred shear force is limited by tensile strength of steel, T or compressive strength of the timber sheathing, C as determined in Equations (1) and (2) respectively;

$T = 900 \times 450 = 405$ kN

$C = 600 \times 45 \times 28 = 756$ kN

Hence, according to Equations (5) and (6), the required number of fasteners to achieve complete shear connection is:

$N_f = 2 \times 405/8 = 101$

The number of ustilised fasteners in the examined system is; $n = 6000/300 = 20$

Therefore, attained degree of shear connection η is: $\eta = 20/101 = 0.2 \leq 1$

Calculation of shear bond coefficient and effective flexural stiffness

This approach is based on Appendix B of Eurocode EN 1995-1-1[40]

$$\gamma = \frac{1}{1 + \frac{\pi^2 S E_t A_t}{K L^2}} \tag{8}$$

γ is a shear bond coefficient, S (spacing of shear connections) = 300 mm, E_t (modulus of elasticity of timber floorboard) = 10,000 MPa, A_t (area of timber floorboard) = $600 \times 45 = 27000$ (mm^2), K (slip modulus) = 10000 N/mm, and L (length of the member) = 6000 mm

From Equation(1), $\gamma = 0.31$

The effective stiffness $(EI)_{eff}$ of the cold-formed steel and timber composite assembly can be determined using Equation (9).

$$(EI)_{eff} = E_t I_t + \gamma E_t A_t a1^2 + E_s I_s + E_s A_s a_2{}^2 \tag{9}$$

a_1 is the distance between the centroid of timber, and the centroid of composite assembly a_2 is the distance between the centroid of CFS and composite assembly

$$a2 = \frac{\gamma E_t A_t (h_s + h_t)}{2(\gamma E_t A_t + E_s A_s)} = 39.4 \text{ mm} \tag{10}$$

$$a1 = \frac{1}{2}(h_s + h_t) - a2 = 84.6 \text{ mm} \tag{11}$$

Hence, $(EI)_{eff} = 2.06 \times 10^{12}$ = N.mm^2

Calculation of bending moment capacity

Accounting for slip at the interface between the cold-formed steel and plywood, the effective bending moment capacity, M, of composite CFST beams with partial shear connection is determined using Equation (12).

$$M = M_{el} - \Delta M \tag{12}$$

M_{el} is the elastic bending capacity of CFST beams with full shear interaction, ΔM is the moment due to slip strain. The ultimate elastic bending moment for a CFST beam exhibiting full shear interaction is determined by selecting the lesser of the values calculated from Equation (13) or Equation (14).

In the event that failure in the CFST beam originates from damage to the plywood,

$$M_{et} = f_{yp} l_t n / y_{el} \tag{13}$$

If the onset of failure in the CFST beam is governed by yielding of the cold-formed steel,

$$M_{el} = f_{ys} l_T / y_{el} \tag{14}$$

Where, y_{el} is the centroid of the composite assembly. To calculate the elastic bending moment capacity, first I_T (transformed section moment of intertia), n (ratio of elastic moduli of steel to plywood (E_s/E_p)) is to be calculated

$$n = \frac{210000}{10000} = 21$$

Centroid of composite assembly can be calculated as below;

$$y_{el} = \frac{y_c A_S + \frac{A_t}{n}\left(h_s + \frac{h_t}{2}\right)}{A_S + \frac{A_t}{n}} = 184.9 \text{ mm}$$

Transformed moment of area is calculated as per Equation (15)

$$I_T = I_s + \frac{b_{eff} t_t^3}{12n} + A_s(y_{el} - y_c)^2 + \frac{A_t}{n}\left(y_{el} - h - \frac{h_t}{2}\right)^2 = 11.1 \text{ x } 10^6 \text{ mm}^4 \quad (15)$$

Hence, elastic ultimate bending moment of CFST beam is, M_{el} = 450x11.1x10^6 / 184.9 = 27.1 kN.m

Moment due to slip strain,

$$\Delta M = \frac{M_{el} h h_s A_s \left(E_S I_T - E I_{eff}\right)}{6 E I_{eff} + h h_s S_s A_s I_T} = 1.3 \text{kN.m}$$

Actual bending moment capacity of composite CFST beam with partial shear connection,

M = 27.1-1.3 = 25.6 kN.m > M_d Ok #

Calculation of shear resistance

The cross-sectional moment capacity of the tested flooring systems can be considerably influenced by the degree of composite action achieved, whereas the shear capacity is determined exclusively by the properties of the bare CFS joist. Per Appendix D of AS 4600[31] , the elastic buckling shear force, V_{cr},for the webs of cold-formed steel members subjected to shear should be calculated using the following expression:

$$V_{cr} = \frac{\pi^2 E A_w k_v}{12\left(1-v^2\right)\left(\frac{d_1}{t}\right)^2}$$

Where, $K_v = K_{ss} + K_n\left(K_{sf} - K_{ss}\right)$

Since, a/d1 = 5000/250 = 20 > 1

K_{ss} = 5.34 + 4/(a/d_1) = 5.54, K_n = 0.23

K_{sf} = 8.98+5.61/(a/d_1)^2 – 1.99/(a/d_1)^3 = 8.99

Hence, K_v = 5.54 + 0.23 ×(8.99-5.54) = 6.33 and $A_w = d_1.t$ = 250 ×2.4 = 600mm^2

V_{cr} = 63270 N = 63.27 kN

As per the clause 7.2.3 of AS 4600, the nominal member shear capacity (Vv) of CFS beams shall be calculated as follows

Since, $\lambda_v = \sqrt{\frac{V_y}{V_{cr}}}$

V_y = 0.6 ×A_w ×f_y = 0.6 ×600 ×450 = 162 kN

λ_v = (162/63.27)^0.5 = 1.6> 1.227, V_v= V_{cr} = 63.27 kN

V_{cr} = 63.27 kN > V_d Ok#

Calculation of deflection

Deflection at midspan for a simply supported beam subjected to a uniformly distributed load q_s* is;

$$\delta_{\max} = \frac{5q_s L^4}{384EI_{\text{eff}}}$$

$\delta_{\max} = 24.5$ mm < Span/240 = 25 mm Ok#

Therefore, the composite beam satisfies the structural requirements for bending, shear, and deflection. The manufacturer's specification lists the moment capacity of the bare steel beam at 18.5 kN·m. Accounting for the shear interaction provided by the mechanical fasteners, the composite system's moment capacity increases to 25.6 kN·m, representing an improvement of 39%. This example clearly demonstrates the significant difference between the bare steel joist and the composite beam, thereby underscoring the importance of considering composite action in CFST flooring systems to fully benefit from enhanced strength and stiffness.

8 Conclusion

This research developed three-dimensional finite element models to simulate the structural behaviour of composite flooring systems comprising cold-formed steel (CFS) joists and timber sheathing. The numerical models were rigorously validated against experimental data presented within this study. Following successful validation across specimens featuring various fastening configurations, parametric analyses were undertaken to evaluate the effects of CFS joist thickness, section depth, and fastener spacing on overall structural performance. Results indicated that increases in joist thickness and depth enhance both the ultimate bending capacity and stiffness, attributable to larger section modulus and moment of inertia values. Moreover, decreasing fastener spacing substantially improves the degree of composite action, thereby increasing flexural stiffness and load capacity.

These outcomes offer valuable guidance for the design and optimisation of lightweight composite floor systems. For example, augmenting joist dimensions is an effective approach for long-span floors to control deflections and satisfy serviceability criteria while minimising material consumption. Adjusting fastener spacing provides a practical and economical strategy to boost composite efficiency without modifying joist geometry. Such findings are pertinent for residential and commercial flooring designs where considerations of weight, cost, and constructability are critical.

Additionally, a formula for calculating shear connector spacing required to achieve full shear interaction is proposed. A simplified design example demonstrates the application of the developed method to estimate bending capacity and deflection, explicitly accounting for shear slip between the composite components. Overall, this design approach offers engineers a robust tool for the efficient design of composite CFST flooring systems.

CRediT authorship contribution statement

Dheeraj Karki: Investigation, Formal analysis, Writing – original draft. **Harry Far**: Conceptualization, Funding acquisition, Supervision, Investigation, Formal analysis, Writing – original draft.

References

[1] Rogan, A., Lawson, R., and Bates-Brkljac, N. J. S. C. I., Ascot, Uk, Value and benefits assessment of modular construction, 2000.

[2] Boyd, N., Khalfan, M. M., and Maqsood, T., Off-site construction of apartment buildings, Journal of architectural engineering 2013; 19(1): 51-57.

[3] Ferdous, W., Bai, Y., Ngo, T. D., Manalo, A., and Mendis, P., New advancements, challenges and opportunities of multi-storey modular buildings – A state-of-the-art review, Engineering Structures 2019; 183: 883-893. https://doi.org/10.1016/j.engstruct.2019.01.061

[4] Loss, C., Piazza, M., and Zandonini, R., Connections for steel–timber hybrid prefabricated buildings. Part I: Experimental tests, Construction and Building Materials 2016; 122: 781-795. https://doi.or g/10.1016/j.con

buildmat.2015.12.002
[5] Ceccotti, A., Composite concrete-timber structures, Progress in Structural Engineering and Materials 2002; 4(3): 264-275.
[6] Karki, D. and Far, H., State of the art on composite cold-formed steel flooring systems, Steel Construction, 2021. https://doi.org/10.1002/stco.202000026
[7] Ellobody, E. and Young, B., Performance of shear connection in composite beams with profiled steel sheeting, Journal of Constructional Steel Research 2006; 62(7): 682-694. https://doi.org/10. 1016/j.jcsr.2005.11.004
[8] Rackham, J. W., Couchman, G. H., and Hicks, S. J., Composite slabs and beams using steel decking: Best practice for design and construction, in "MCRMA Technical paper No.13," Steel Construction Institute2009.
[9] Deam, B. L., Fragiacomo, M., and Buchanan, A. H., Connections for composite concrete slab and LVL flooring systems, Material and Structures, journal article 2008; 41(3): 495-507.1617/s11527-007-9261-x
[10] Lukaszewska, E., Fragiacomo, M., and Johnsson, H., Laboratory Tests and Numerical Analyses of Prefabricated Timber-Concrete Composite Floors, Journal of structural engineering 2010; 136(1): 46-55.doi: 10.1061/(ASCE)ST.1943-541X.0000080
[11] Hassanieh, A., Valipour, H. R., and Bradford, M. A., Composite connections between CLT slab and steel beam: Experiments and empirical models, Journal of Constructional Steel Research 2017; 138: 823-836. https://doi.org/10.1016/j.jcsr.2017.09.002
[12] Loss, C. and Davison, B., Innovative composite steel-timber floors with prefabricated modular components, Engineering Structures 2017; 132: 695-713. https://doi.org/10.1016/j.en gstruct.2016.11.062
[13] Zhou, X., Shi, Y., Xu, L., Yao, X., and Wang, W., "A simplified method to evaluate the flexural capacity of lightweight cold-formed steel floor system with oriented strand board subfloor," Thin-Walled Structures 2019; 134: 40-51. 1016/j.tws.2018.09.006
[14] Xu, L. and Tangorra, F. M., Experimental investigation of lightweight residential floors supported by cold-formed steel C-shape joists, Journal of Constructional Steel Research 2007; 63(3): 422-435. 1016/j.jcs r.20 06.05.010
[15] Kyvelou, P., Gardner, L., and Nethercot, D. A., Testing and Analysis of Composite Cold-Formed Steel and Wood−Based Flooring Systems, Journal of Structural Engineering 2017; 143(11):1061. (ASCE)st. 1943-541 x.0001885
[16] Kyvelou, P., Gardner, L., and Nethercot, D. A., Finite element modelling of composite cold-formed steel flooring systems, Engineering Structures2018; 158: 28-42. 1016/j.engstruct.2017.12.024
[17] Parnell, R., Davies, B. W., and Xu, L., Vibration Performance of Lightweight Cold-Formed Steel Floors, Journal of structural engineering 2010; 136: 645-653.10.1061/(ASCE)ST.1943-541X.0000168
[18] Kankanamge, N. D. and Mahendran, M., Behaviour and design of cold-formed steel beams subject to lateral–torsional buckling, Thin-Walled Structures 2012; 51: 25-38. https://doi.org/10.1016/j.t ws.2011.10. 012
[19] Karki, D., Far, H., and Saleh, A., Numerical Studies into Factors Affecting Structural Behaviour of Composite Cold-Formed Steel and Timber Flooring Systems, Journal of Building Engineering 2021; 102692. https://doi.org/10.1016/j.jobe.2021.102692
[20] Far, H., Flexural Behavior of Cold-Formed Steel-Timber Composite Flooring Systems, Journal of structural engineering 2020; 146(5): 06020003. https://doi. org/10.1061/(ASCE)ST.1943-541X.0002600
[21] Navaratnam, S. et al., Development of cross laminated timber-cold-formed steel composite beam for floor system to sustainable modular building construction, Structures 2021; 32: 681-690. https://doi. org/10.101 6/j.istruc.2021.03.051
[22] Kyvelou, P., Reynolds, T. P. S., Beckett, C. T. S., and Huang, Y., Experimental investigation on composite panels of cold-formed steel and timber, Engineering Structures 2021; 247: 113186. https://doi. org/10.1016/ j.engstruct.2021.113186
[23] Karki, D., Al-Hunaity, S., Far, H., and Saleh, A., Composite connections between CFS beams and plywood panels for flooring systems: Testing and analysis, Structures 2022; 40: 771-785. https://doi.org/10.1016/j.is truc.2022.04.064
[24] Karki, D., Far, H., and Al-Hunity, S., Determination of Slip Modulus of Cold Formed Steel Composite Members Sheathed with Plywood Structural Panels, Steel and Composite Structures: an international journal 2022; 43: 511-522. https://doi.org/10.12989/scs.2022.43.4.511
[25] Karki, D., Far, H., and Nejadi, S., Structural Behavior of Prefabricated Composite Cold-Formed Steel and Timber Flooring Systems, Journal of Structural Engineering 2024; 150(7): 04024065. 1061/JSENDH.STEN G-12382
[26] Ansys Inc., Theory Reference for the Mechanical APDL and Mechanical Applications, ed: Ansys Incorporation, Canonsburg, PA, 2009.
[27] Majdi, Y., Hsu, C.-T. T., and Zarei, M., Finite element analysis of new composite floors having cold-formed steel and concrete slab, Engineering Structures 2014; 77: 65-83. https://doi.org/10.1016/j.engstruct.2014. 0 7.030

[28] Wang, H. and Zhang, Y., Experimental and numerical investigation on cold-formed steel C-section flexural members, Journal of Constructional Steel Research 2009; 65(5): 1225-1235. https: //doi.org/10.1016/j.jcsr. 2008.08.007
[29] Pham, C. H. and Hancock, G. J., Numerical simulation of high strength cold-formed purlins in combined bending and shear, Journal of Constructional Steel Research 2010; 66(10): 1205-1217. https://d oi.org/10.1 016/j.jcsr.2010.04.014
[30] Schafer, B. W. and Pekoz, T., Computational modelling of cold-formed steel characterising geometric imperfections and residual stresses, Journal of Constructional Steel Research 1998; 47: 193-210.
[31] Standard Australia, AS/NZS: 4600-2018 Cold-formed steel structures, SAI Global, 2018.
[32] Al-Hunaity, S. A., Karki, D., and Far, H., Shear connection performance of cold-formed steel and plywood composite flooring systems: Experimental and numerical investigation, Structures 2023; 4(8): 901-917.https://doi.org/10.1016/j.istruc.2023.01.008
[33] Arriaga-Martitegui, F., Peraza-Sánchez, F., and García-Esteban, L., Characteristic values of the mechanical properties of radiata pine plywood and the derivation of basic values of the layers for a calculation method, Biosystems Engineering 2008; 99(2) 256-266. 2008. https://doi.org/10.1016/j. biosystems eng.2007.10.004
[34] Xu, L., Sultana, P., and Zhou, X., "Flexural strength of cold-formed steel built-up box sections," Thin-Walled Structures 2009; 47(6): 807-815. https://doi.org/10.1016/j.tws.2009.01.005
[35] Ren, W.-X., Fang, S.-E., and Young, B., Analysis and design of cold-formed steel channels subjected to combined bending and web crippling, Thin-Walled Structures 2006; 44(3): 314-320. https://d oi.org/10.10 16/j.tws.2006.03.009
[36] Case, THIN WALL 2, A Computer Program for Cross-section Analysis and Finite Strip Buckling Analysis and Direct Strength Design of Thin-walled Structures, ed. Centre for Advanced Structural Engineering, School of Civil Engineering, The University of Sydney, 2006.
[37] Shi, Y., Yang, K., Guan, Y., Yao, X., Xu, L., and Zhang, H., The flexural behavior of cold-formed steel composite beams, Engineering Structures 2020; 218: 110819. https://doi.org/10.1016/j.engstr uct.2020. 110 819
[38] Standard Australia, AS/NZS 2327:2017 Composite Structures-Composite steel-concrete construction in buildings, SAI Global, 2017.
[39] Kyvelou, P., Gardner, L., and Nethercot, D. A., Design of Composite Cold-Formed Steel Flooring Systems, Structures 2017; 12: 242-252. 1016/j.istruc.2017.09.006
[40] Cen, EN 1995-1-1:2004 Eurocode 5: Design of timber structures-Part 1-1: General-Common rules and rules for buildings, European Committee for Standardization, 2004.